Nanoscale Research Letters
a SpringerOpen Journal

NANO EXPRESS Open Access

Near-infrared quantum cutting in Ho^{3+}, Yb^{3+}-codoped $BaGdF_5$ nanoparticles via first- and second-order energy transfers

Linna Guo, Yuhua Wang*, Jia Zhang, Yanzhao Wang and Pengyu Dong

Abstract

Infrared quantum cutting involving Yb^{3+} 950–1,000 nm ($^2F_{5/2} \rightarrow {}^2F_{7/2}$) and Ho^{3+} 1,007 nm ($^5S_2, {}^5F_4 \rightarrow {}^5I_6$) as well as 1,180 nm ($^5I_6 \rightarrow {}^5I_8$) emissions is achieved in $BaGdF_5$: Ho^{3+}, Yb^{3+} nanoparticles which are synthesized by a facile hydrothermal route. The mechanisms through first- and second-order energy transfers were analyzed by the dependence of Yb^{3+} doping concentration on the visible and infrared emissions, decay lifetime curves of the $^5F_5 \rightarrow {}^5I_8$, $^5S_2/{}^5F_4 \rightarrow {}^5I_8$, and $^5F_3 \rightarrow {}^5I_8$ of Ho^{3+}, in which a back energy transfer from Yb^{3+} to Ho^{3+} is first proposed to interpret the spectral characteristics. A modified calculation equation for quantum efficiency of Yb^{3+}-Ho^{3+} couple by exciting at 450 nm was presented according to the quantum cutting mechanism. Overall, the excellent luminescence properties of $BaGdF_5$: Ho^{3+}, Yb^{3+} near-infrared quantum cutting nanoparticles could explore an interesting approach to maximize the performance of solar cells.

Keywords: Near infrared quantum cutting, First- and second-order energy transfers, Back energy transfer, $BaGdF_5$: Ho^{3+}, Yb^{3+}

Background

Lanthanide (Ln) ions could exhibit both efficient upconversion (UC) and downconversion (DC) emission properties [1], where the UC process converts low-energy light, usually near infrared (NIR) or infrared, to higher energies, ultraviolet or visible, via multiple absorptions or energy transfers (ETs). In contrast, DC process is the conversion of higher-energy photons into lower-energy photons [2]. For the time being, DC of NIR luminescence (i.e., NIR quantum cutting (QC)), which downconverts one incident UV-blue photon into two NIR photons (approximately 1,000 nm), has attracted more attention for their application in silicon solar cells by modifying the incident light wavelength [3].

As it is well known to us that the solar spectrum and the bandgap energy of silicon semiconductor do not match each other, thus photons with energy lower than the bandgap could not be absorbed, while for photons with energy larger than the bandgap, the excess energy is lost by thermalization of hot charge carriers [4]. Take these sources of energy loss into account for the solar spectrum; the maximum energy efficiency is 30% only for a crystalline Si solar cell with a bandgap of 1.12 eV [3]. Considering this, if the conversion of one UV or visible photon into two NIR photons with energies about 1.12 eV is realized through QC in a silicon solar cell, the energy loss related to thermalization of hot charge carriers can be reduced, and the solar cell efficiency will be enhanced greatly to satisfy the application requirement [5].

To obtain high NIR QC efficiency, other Ln^{3+} ions are generally codoped with Yb^{3+} in the hosts, and it is commonly demonstrated in Ln^{3+}-Yb^{3+} (Ln = Tb, Tm, Pr, Er, Nd, and Ho) couple-codoped materials [6]. Generally speaking, there are two mechanisms involved in the NIR QC in Ln^{3+}-Yb^{3+} couple [5]: one is second-order cooperation of energy transfer (CET) based on one donor and two acceptor ions, and the other is first-order resonance energy transfer (ET). Nevertheless, CET process is not as efficient as resonance ET [7-9], but high CET efficiency would be realized at high Yb^{3+} concentration. Thus, a NIR QC via resonant first-order ET process seems more favorable for luminescent materials, which

* Correspondence: wyh@lzu.edu.cn
Department of Materials Science, School of Physical Science and Technology, Lanzhou University, Lanzhou 730000, People's Republic of China

requires an intermediate energy level of donor ion to resonantly excite acceptor ions by a two-step ET process. There are many reports about second-order CET [2,10-14]; however, there are few reports about first- and second-order ETs occurring simultaneously in one research system.

On the other hand, to fulfill the requirements of NIR QC, host materials should have the energy of phonons as low as possible in order to reduce probabilities of multiphonon relaxations between spaced energy levels of Ln^{3+} ions. Cubic $BaGdF_5$, a tri-fluoride compound, has a wide bandgap and low phonon energy which is a suitable NIR QC matrix [15]. Meanwhile, Ho^{3+} ion has favorable metastable energy levels and considerable energy match between Yb^{3+} and Ho^{3+}, so Ho^{3+}/Yb^{3+} couple could be a good choice in NIR QC investigation. However, NIR QC reports in Ho^{3+}/Yb^{3+}-codoped materials are limited in $NaYF_4$ and glass ceramic [7,9]. In addition, considering NIR nanomaterials is convenient in the practical application of the coating for the solar cells. Herein, we prepared $BaGdF_5$: Ho^{3+}, Yb^{3+} nanoparticles with different Yb^{3+} concentrations by a trisodium citrate (Cit^{3-})-assisted hydrothermal method, which is less finicky, low-cost, and effective for large-scale production. Furthermore, NIR QC via first- and second-order resonant ET processes and a back ET from Yb^{3+} to Ho^{3+} in $BaGdF_5$: Ho^{3+}, Yb^{3+} nanoparticles is firstly investigated, and the corresponding quantum efficiencies (QE) are also calculated.

Methods

$BaGd_{1-0.01-x\%}Yb_{x\%}Ho_{0.01}F_5$ ($0 \le x \le 20$) samples were prepared by a hydrothermal process. Firstly, 1 mmol rare earth oxides Gd_2O_3, Yb_2O_3, and Ho_2O_3 were dissolved in dilute HNO_3 solution, and the residual HNO_3 was removed by heating and evaporation, resulting in the formation of clear solution of $RE(NO_3)_3$ (RE = Gd, Yb, Ho). Cit^{3-} aqueous solution was added into the $Ba(NO_3)_2{\cdot}2H_2O$ and $RE(NO_3)_3$ solution to form metal-Cit complex. After vigorous stirring for 30 min, aqueous solution containing 4 mmol $NaBF_4$ was poured into the above solution, and pH value of the mixture was adjusted to about 4.5 by adding diluted HCl or $NH_3{\cdot}H_2O$. After additional agitation for 15 min, the as-obtained mixed solution was transferred into a 50-ml teflon autoclave, which was tightly sealed and maintained at 180°C for 24 h. As the autoclave was cooled to room temperature naturally, the resulting precipitates were separated via centrifugation, dried in oven at 80°C for 12 h.

Characterizaton

The XRD patterns were obtained on Rigaku D/max-2400 powder diffractometer (Rigaku Corporation, Tokyo, Japan) using Cu Kα radiation (1.5405 Å) at 40 kV and 60 mA. The size, shape, and structure of the as-prepared samples were characterized by SEM (S-4800). Emission and excitation measurements were performed using an Edinburgh Instruments' FLS920 fluorescence spectrometer (Livingston, UK), and a 0.3-m double excitation monochromator and two emission monochromators to record the emission spectra in the wavelength range of 200–850 nm (with a Hamamatsu R928 photomultiplier tube, Bridgewater, NJ, USA) or in the wavelength range of 850–1650 nm (with a liquid nitrogen-cooled Hamamatsu R5509-72 PMT). All spectra were measured at room temperature.

Results and discussion

The XRD patterns and representative SEM photograph of $BaGd_{1-0.01-x\%}Yb_{x\%}Ho_{0.01}F_5$ ($0 \le x \le 20$) nanoparticles are shown in Figure 1a, b, respectively. It is obvious that the locations and relative intensities of the diffraction peaks coincide well with the data reported in the JCPDS standard card (no. 24–0098). No additional peaks of other phases were found, indicating that the pure-phase $BaGdF_5$ is obtained. It can be seen from Figure 1b that the nanoparticles are relatively dispersed with uniform granular morphology and sizes which are about 40 nm.

Photoluminescence excitation (PLE) spectra monitoring at 540 nm and photoluminescence (PL) spectra in the visible region under 450-nm excitation of $BaGdF_5$: 1% Ho^{3+}, x% Yb^{3+} ($0 \le x \le 20$) nanoparticles were investigated, as shown in Figure 2a,b, respectively. It is noticed from Figure 2a that the most intense excitation band of Ho^{3+} is at 450 nm, corresponding to the $^5I_8 \rightarrow {}^5G_6$, $^5F_1$ transition of Ho^{3+} ions. Figure 2b shows the emission peaks of Ho^{3+} at about 483, 545, 651, and 747 nm which are attributed to the $^5F_3 \rightarrow {}^5I_8$, $^5F_4/{}^5S_2 \rightarrow {}^5I_8$, $^5F_5 \rightarrow {}^5I_8$, and $^5S_2 \rightarrow {}^5I_7$ transitions of Ho^{3+}, respectively [16,17]. It is worthwhile pointing out that both the excitation and emission intensities decrease with increasing Yb^{3+} concentration, which may be due to the Ho^{3+} transferring its energy to the Yb^{3+}, but it needs more evidence to testify this guess, which will be discussed as follows:

PLE spectra of $BaGdF_5$: 1% Ho^{3+}, x% Yb^{3+} ($0 \le x \le 20$) nanoparticles are also recorded by monitoring the characteristic emission of Yb^{3+} at 980 nm (Figure 3a). The presence of Ho^{3+} excitation in the PLE spectra of $BaGdF_5$: 1% Ho^{3+}, x% Yb^{3+} by monitoring the characteristic emission of Yb^{3+} gives an evidence to the energy transfer from Ho^{3+} to Yb^{3+}. Furthermore, it is noteworthy that a broad emission band in the range of 950–1,100 nm, corresponding to the $^2F_{5/2} \rightarrow {}^2F_{7/2}$ transition of Yb^{3+} and $^5S_2$,$^5F_4 \rightarrow {}^5I_6$ transition of Ho^{3+} ions, has also been observed under the Ho^{3+} excitation at 450 nm

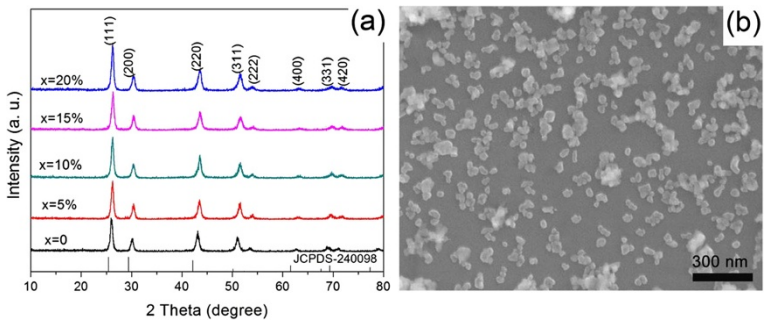

Figure 1 XRD patterns and SEM image. (**a**) The measured XRD patterns of $BaGdF_5$: 1%Ho^{3+}, *x*%Yb^{3+} ($0 \le x \le 20$) as well as the standard XRD pattern of $BaGdF_5$ (JCPDS no. 24–0098) used as a reference. (**b**) SEM image of $BaGdF_5$: 1%Ho^{3+} nanoparticle as a representative.

(as shown in Figure 3b). This is another evidence of ET from Ho^{3+} to Yb^{3+}. Simultaneously, the 1,180-nm emission due to $^5I_6 \rightarrow {}^5I_8$ transition of Ho^{3+} is also detected. NIR emission intensity of Yb^{3+} intensifies rapidly with increasing Yb^{3+} concentration from 0 to 15 mol%. Whereas, 1,180-nm emission intensity of Ho^{3+} enhances with increasing Yb^{3+} concentration even when Yb^{3+} concentration is 20 mol%. That is to say, the NIR emission quenching concentration of Ho^{3+} is higher than that of Yb^{3+}. The reasons for the above phenomenon will be discussed later.

For excitation at 450 nm, there are three possible ET processes from Ho^{3+} to Yb^{3+} responsible for the NIR emission of Yb^{3+} ions, in view of energy levels of Ho^{3+} xand Yb^{3+} ions (shown in Figure 4) [18,19]. (1) Ho^{3+}: $^5F_3 \rightarrow {}^5I_8$ transition is located at approximately twice the energy of the Yb^{3+}: $^2F_{5/2} \rightarrow {}^2F_{7/2}$ transition, which in theory can transfer its energy to Yb^{3+} ions through a CET mechanism: $Ho^{3+}(^5F_3) \rightarrow 2Yb^{3+}(^2F_{5/2}) + h\nu$; (2) Ho^{3+} ion could relax from its $^5S_2$, $^5F_4$ to $^5I_6$ level and then transfer its energy to only one Yb^{3+} ion, which belongs to first-order resonance CR1 process ($^5S_2$, $^5F_4$(Ho) + $^2F_{7/2}$(Yb) $\rightarrow$ $^5I_6$ (Ho) + $^2F_{7/2}$(Yb) + $h\nu$; and (3) similarly, CR2 process: $^5F_5$(Ho) + $^2F_{7/2}$(Yb) $\rightarrow$ $^5I_7$(Ho) + $^2F_{7/2}$ (Yb) + $h\nu$.

According to the above mechanisms, the emission of Ho^{3+}: $^5I_6 \rightarrow {}^5I_8$ is mainly followed by the occurrence of CR1 process. Also, as it is well known to us that CET process is not efficient at lower Yb^{3+} content due to its intrinsic nature, but at a relatively high Yb^{3+} concentration of 15 mol%, the CET process could become efficient, and this efficiency (η_{CET}) can be estimated by Equation 1: [11]

$$\eta_{ET} = \eta_{x\%Yb} = 1 - \frac{\int I_{x\%Yb}dt}{\int I_{0\%Yb}dt} \quad (1)$$

where I denotes the decay intensity, and *x*% Yb denotes the Yb^{3+} contents. To determine the η_{CET} for $BaGdF_5$: 1% Ho^{3+}, *x*% Yb^{3+} ($0 \le x \le 15$) nanoparticles, a series of

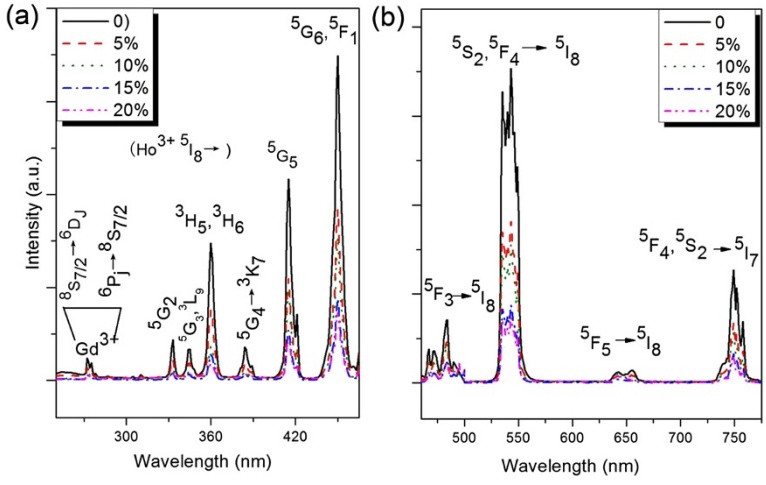

Figure 2 PLE and PL spectra by monitoring Ho^{3+} emission. (**a**) PLE spectra by monitoring Ho^{3+}: $^5S_2 \rightarrow {}^5I_8$ emission at 540 nm and (**b**) visible PL spectra under excitation of 450 nm ($^5I_8 \rightarrow {}^5G_6$, $^5F_1$) of $BaGdF_5$: 1% Ho^{3+}, *x*% Yb^{3+} ($0 \le x \le 20$) nanoparticles.

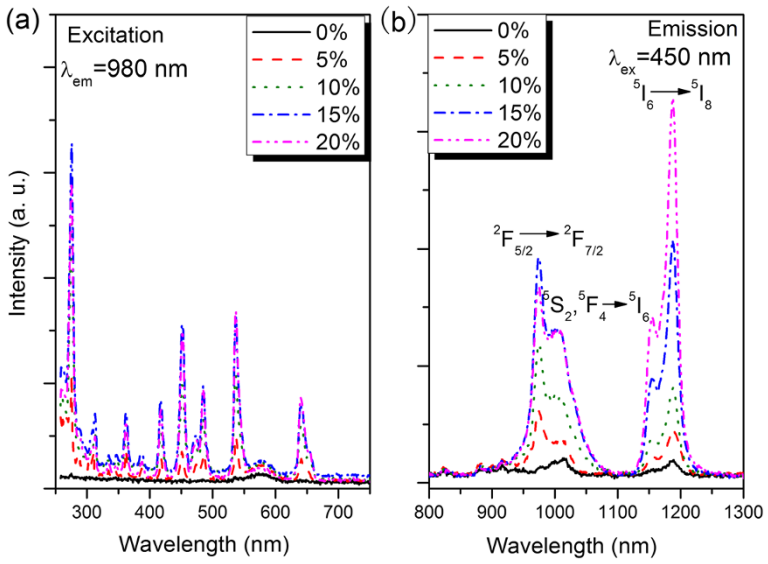

Figure 3 PLE and PL spectra monitoring of the Yb^{3+} emission. (**a**) PLE spectra monitoring of the Yb^{3+}: $^2F_{5/2} \rightarrow {}^2F_{7/2}$ emission and (**b**) PL spectra in the infrared region under excitation of 450 nm ($^5I_8 \rightarrow {}^5G_6$, $^5F_1$) of $BaGdF_5$: 1% Ho^{3+}, *x*% Yb^{3+} ($0 \le x \le 20$) nanoparticles.

decay curves of Ho^{3+}: $^5F_3 \rightarrow {}^5I_8$ emissions at 486 nm are determined, as shown in Figure 5a. All the decay curves demonstrate double-exponential feature (Table 1), so the decay times can be determined using a curve fitting technique based on the following equation:

$$I = A_1 \exp\left(-\frac{t}{\tau_1}\right) + A_2 \exp\left(-\frac{t}{\tau_2}\right) \quad (2)$$

where I is phosphorescence intensity; A_1 and A_2, constants; t, time; and τ_1 and τ_2, decay constants deciding the rates for the rapid and the slow exponentially decay components, respectively. The average decay times (τ) can be calculated by the following formula:

$$< \tau >= \left(A_1\tau_1^2 + A_2\tau_2^2\right)/(A_1\tau_1 + A_2\tau_2) \quad (3)$$

Also, the corresponding lifetime values as well as η_{CET} are calculated, which are summarized in the inset of Figure 5a. Unexpectedly, η_{CET} is calculated to be as high as 92% in the $BaGdF_5$: 1% Ho^{3+}, 15% Yb^{3+}. In this case, the number of the remaining photons relaxed to the

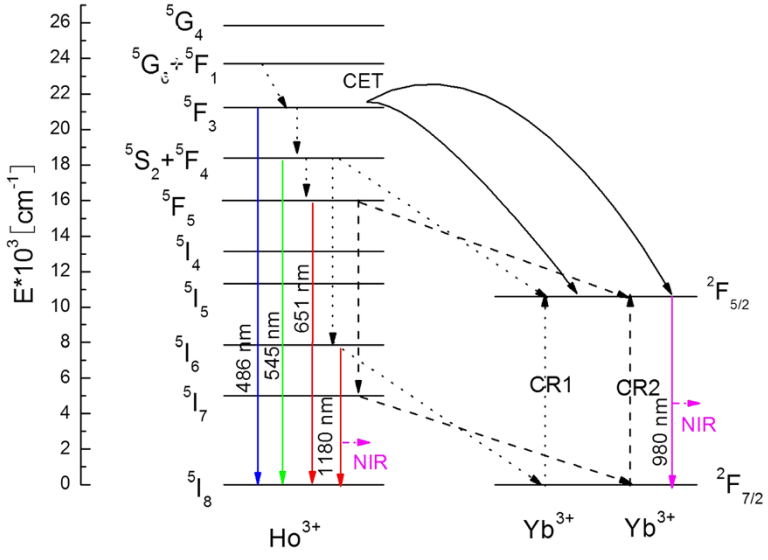

Figure 4 Energy level diagram of Ho^{3+} and Yb^{3+} showing possible mechanisms for a NIR QC processes.

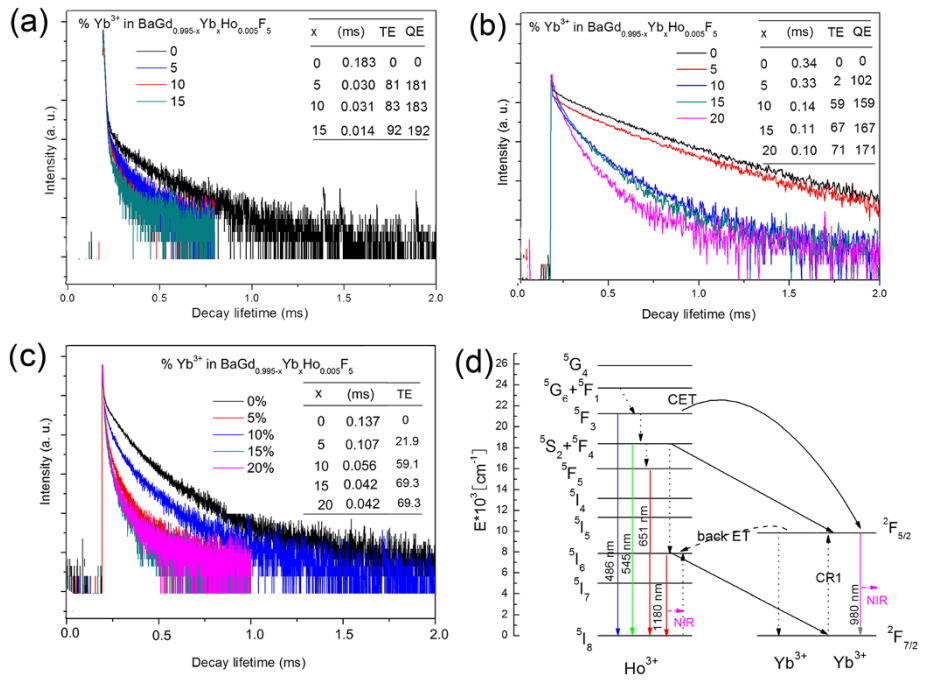

Figure 5 Decay curves of Ho^{3+}. For (**a**) $^5F_3 \rightarrow {}^5I_8$, (**b**) $^5F_4$, $^5S_2 \rightarrow {}^5I_8$, and (**c**) $^5F_5 \rightarrow {}^5I_8$ emissions under excitation of 450 nm. The inset shows the average decay lifetime and energy transfer efficiency as a function of Yb^{3+} doping concentration. (**d**) Energy level diagram of Ho^{3+} and Yb^{3+} showing mechanisms for NIR QC processes.

lower energy levels than $^5F_3$ to give other emission is very small. Besides, double-exponential decay curves of Ho^{3+}: $^5F_4$, $^5S_2 \rightarrow {}^5I_8$ emission at 545 nm as well as $^5F_5 \rightarrow {}^5I_8$ emission at 651 nm with logarithmic coordinates are plotted with various Yb^{3+} concentrations in Figure 5b, c, and the highest resonant ET efficiencies for CR1(η_{CR1}) and CR2(η_{CR2}) are calculated to be 71% and 69%, respectively, which are also efficient. All the above results just indicate that the Yb^{3+}: $^2F_{5/2} \rightarrow {}^2F_{7/2}$ emission should demonstrate stronger intensity and higher quenching concentration than those of Ho^{3+}: $^5I_6 \rightarrow {}^5I_8$ emission.

However, the NIR emission spectra in Figure 3 show distinct results. Based on these experimental

Table 1 The fitting results of parameters of the double-exponential decays

Monitoring wavelength	Yb^{3+} concentration (mol%)	τ_1 (μs)	A_1	τ_2 (μs)	A_2	X^2
486 nm ($^5F_3 \rightarrow {}^5I_8$)	0	23.0494	127.162	204.1946	110.036	1.493
	5	6.2807	1,731.739	68.1584	117.146	1.521
	10	6.1677	4,114.752	82.2261	152.536	1.397
	15	5.0831	4,341.002	49.8707	105.941	1.558
	20	5.1521	1,799.106	34.5770	74.643	1.500
545 nm ($^5S_2 \rightarrow {}^5I_8$)	0	143.0003	2,221.670	399.7964	2,634.467	1.473
	5	106.2121	1,454.757	378.4078	2,065.503	1.359
	10	60.6316	2,270.273	199.2826	885.756	1.612
	15	50.8624	2,892.493	166.1588	1,010.801	1.539
	20	52.5225	666.286	152.9727	282.404	1.484
651 nm ($^5F_5 \rightarrow {}^5I_8$)	0	68.2479	1,422.916	206.0216	472.991	1.421
	5	38.4695	903.197	157.5332	307.477	1.576
	10	18.9739	650.965	87.4463	170.137	1.496
	15	14.1099	691.857	71.4125	126.626	1.528
	20	138.514	669.904	67.1548	151.641	1.416

results and combining the energy levels of Yb^{3+} and Ho^{3+}, we brought up a novelty back ET process from Yb^{3+} to Ho^{3+} ($Yb^{3+}(^2F_{5/2}) + Ho^{3+}(^5I_8) \rightarrow Yb^{3+}(^2F_{7/2}) + Ho^{3+}(^5I_6) + h\nu$) which may be occurring in the NIR QC system, as shown in the Figure 5d, since the back ET phenomenon widely exists in UC for Yb^{3+}, Ho^{3+}-doped materials [20,21]. This ET not only increases the Ho^{3+}: $^5F_5 \rightarrow {}^5I_8$ emission intensity but also reduces the Yb^{3+}: $^2F_{5/2} \rightarrow {}^2F_{7/2}$ emission intensity, resulting in the spectral features in Figure 3.

The QE is known to be defined as the ratio of the number of photons emitted to the number of photons that are absorbed. It can be concluded from Figure 5d that the extra photons emitted come only by CET and CR1 process for every phonon absorbed when excited at 450 nm. Therefore, supposing that all the excited Yb^{3+} and the residual excited Ho^{3+} decay radiatively, a modified calculation equation for the total QE (η_{QE}) when excited at 450 nm can be theoretically expressed as follows according to [11]:

$$\eta_{QE} = 1 + \eta_{CET} + (1 - \eta_{CET})\eta_{CR1}$$

where the last two terms stand for the extra QEs for CTE and CR1 processes, respectively. The total η_{QE} for $BaGdF_5$: 15% Yb^{3+}, 1% Ho^{3+} is calculated to 192% by this formulation. This so high QE partly results from the Ho^{3+} $^5I_6$-$^5I_8$ emission (1,180 nm), which is useless to enhance the efficiency of Si solar cells, since this emission does not match the spectral response of Si solar cells.

Conclusions

Unlike the common situation that two emitting photons are from the acceptor Yb^{3+} ions, both the donor (Ho^{3+}) and the acceptor (Yb^{3+}) could emit NIR photons under blue light excitation. The visible emissions decrease with the introduction of the Yb^{3+} ions, while the NIR emissions at 980 nm and 1,180 nm are greatly enhanced. The quenching concentration of Ho^{3+} is higher than that of Yb^{3+}. The fluorescence decay lifetimes of $^5F_3 \rightarrow {}^5I_8$, $^5F_4$, $^5S_2 \rightarrow {}^5I_8$, and $^5F_5 \rightarrow {}^5I_8$ emissions of Ho^{3+} donors were recorded and calculated as a function of Yb^{3+} concentration. It could be concluded that NIR emissions are mainly through second- and first-order ET processes: $Ho^{3+}(^5F_3) \rightarrow 2Yb^{3+}(^2F_{5/2}) + h\nu$, $Ho^{3+}(^5S_2) + Yb^{3+}(^2F_{7/2}) \rightarrow Ho^{3+}(^5I_6) + Yb^{3+}(^2F_{5/2}) + h\nu$ by spectra and decay curve analysis. The corresponding QE are calculated to be 192% in $BaGdF_5$: 1% Ho^{3+}, 15% Yb^{3+}, so $BaGdF_5$: Ho^{3+}, Yb^{3+} nanoparticles could open up an approach in designing ultra-efficient photonic devices, for the application in low bandgap solar cells and thermophotovoltaic energy conversion, etc.

Competing interests

The authors declare that they have no competing interests.

Authors' contributions

LG participated in the design of the study, carried out the total experiments, and performed the result analysis, as well as drafted the manuscript. YhW participated in the design of the study, gave the theoretical and experimental guidance, and made the corrections of manuscript. JZ mainly helped in the experiments and measurements. YzW and PD gave the theoretical and experimental guidance and helped amend the manuscript. All authors read and approved the final manuscript.

Authors' information

LG, JZ, YzW, and PD are all Ph.D. candidates, and YhW is a Distinguished Young Scholar at the Department of Materials Science, School of Physical Science and Technology, Lanzhou University.

Acknowledgments

This work is supported by the National Science Foundation for Distinguished Young Scholars (no. 50925206). We express thanks to professor Xueyuan Chen and doctor Haomiao Zhu of the Fujian Institute of Research on the Structure of Matter for their assistance in measuring the luminescence spectra.

Received: 5 October 2012 Accepted: 9 November 2012
Published: 22 November 2012

References

1. Li ZQ, Zhang Y: **Facile synthesis of lanthanide nanoparticles with paramagnetic, down- and up-conversion properties.** *Nanoscale* 2010, **2**:1240–1243.
2. Chen DQ, Yu YL, Wang YS, Huang P, Weng FY: **Cooperative energy transfer up-conversion and quantum cutting down-conversion in Yb^{3+}: TbF_3 nanocrystals embedded glass ceramics.** *J Phys Chem C* 2009, **113**:6406–6410.
3. van der Ende BM, Aarts L, Meijerink A: **Near-infrared quantum cutting for photovoltaics.** *Adv Mater* 2009, **21**:3073–3077.
4. Trupke T, Green MA, Würfel P: **Improving solar cell efficiencies by down-conversion of high-energy photons.** *J Appl Phys* 2002, **92**:1668–1674.
5. Richards BS: **Luminescent layers for enhanced silicon solar cell performance: down-conversion.** *Sol Energy Mater Sol Cells* 2006, **90**:1189–1207.
6. Zhang QY, Huang XY: **Recent progress in quantum cutting phosphors.** *Prog Mater Sci* 2010, **55**:353–427.
7. Lin H, Chen D, Yu Y, Yang A, Wang Y: **Near-infrared quantum cutting in Ho^{3+}/Yb^{3+} codoped nanostructured glass ceramic.** *Opt Lett* 2011, **36**:876–878.
8. van Wijngaarden JT, Scheidelaar S, Vlugt TJH, Reid MF, Meijerink A: **Energy transfer mechanism for downconversion in the (Pr^{3+}, Yb^{3+}) couple.** *Phy Rev B* 2010, **81**:155112-1–155112-6.
9. Deng KM, Gong T, Hu LX, Wei XT, Chen YH, Yin M: **Efficient near-infrared quantum cutting in $NaYF_4$: Ho^{3+}, Yb^{3+} for solar photovoltaics.** *Opt Express* 2011, **19**:1749–1754.
10. Ye S, Zhu B, Luo J, Chen J, Lakshminarayana G, Qiu J: **Enhanced cooperative quantum cutting in Tm^{3+}- Yb^{3+} codoped glass ceramics containing LaF_3 nanocrystals.** *Opt Express* 2008, **16**:8989–8994.
11. Vergeer P, Vlugt TJH, Kox MHF, Den Hertog MI, van der Eerden JPJM, Meijerink A: **Quantum cutting by cooperative energy transfer in $Yb_xY_{1-x}PO_4$:Tb^{3+}.** *Phys Rev B* 2005, **71**:014119-1–014119-11.
12. Zhang QY, Yang CH, Jiang ZH: **Concentration-dependent near-infrared quantum cutting in $GdBO_3$:Tb^{3+},Yb^{3+} nanophosphors.** *Appl Phys Lett* 2007, **90**:061914-1–061914-3.
13. Zhang QY, Yang GF, Jiang ZH: **Cooperative downconversion in $GdAl_3(BO_3)_4$:RE^{3+},Yb^{3+} (RE = Pr, Tb, and Tm).** *Appl Phys Lett* 2007, **91**:051903-1–051903-3.
14. Chen JD, Guo H, Li ZQ, Zhang H, Zhuang YX: **Near-infrared quantum cutting in Ce^{3+}, Yb^{3+} co-doped YBO_3 phosphors by cooperative energy transfer.** *Opt Mater* 2010, **32**:998–1001.
15. Yang DM, Li CX, Li GG, Shang MM, Kang XJ, Lin J: **Colloidal synthesis and remarkable enhancement of the upconversion luminescence of $BaGdF_5$: Yb^{3+}/Er^{3+} nanoparticles by active-shell modification.** *J Mater Chem* 2011, **21**:5923–5927.

16. Capobianco JA, Boyer JC, Vetrone F, Speghini A, Bettinelli M: **Optical spectroscopy and upconversion studies of Ho^{3+}-doped bulk and nanocrystalline Y_2O_3.** *Chem Mater* 2002, **14:**2915–2921.
17. An LQ, Zhang J, Liu M, Wang SW: **Preparation and upconversion properties of Yb^{3+}, Ho^{3+}: Lu_2O_3 nanocrystalline powders.** *J Am Ceram Soc* 2005, **88:**1010–1012.
18. Wang H, Tu C, You Z, Yang F, Wei Y, Wang Y, Li J, Zhu Z, Jia G, Lu X: **Conversion of infrared radiation into visible emission in $NaGd(WO_4)_2$:Yb^{3+}, Ho^{3+} crystals.** *Appl Phys B* 2007, **88:**57–60.
19. Yu DC, Huang XY, Ye S, Zhang QY: **Efficient first-order resonant near-infrared quantum cutting inβ-$NaYF_4$:Ho^{3+}, Yb^{3+}.** *J Alloys Compond* 2011, **509:**9919–9923.
20. Wang F, Liu XG: **Upconversion multicolor fine-tuning: visible to near-infrared emission from lanthanide-doped $NaYF_4$ nanoparticles.** *J Am Chem Soc* 2008, **130:**5642–5643.
21. De la Rosa E, Salas P, Desirena H, Angeles C, Rodríguez RA: **Strong green upconversion emission in ZrO_2:Yb^{3+}–Ho^{3+} nanocrystals.** *Appl Phys Lett* 2005, **87:**241912-1–241912-3.

doi:10.1186/1556-276X-7-636
Cite this article as: Guo *et al.*: Near-infrared quantum cutting in Ho^{3+}, Yb^{3+}-codoped $BaGdF_5$ nanoparticles via first- and second-order energy transfers. *Nanoscale Research Letters* 2012 **7**:636.